

PAPER

# Effect of Co and Mg doping at Cu site on structural, magnetic and dielectric properties of $\alpha$ -Cu<sub>2</sub>V<sub>2</sub>O<sub>7</sub>

To cite this article: Abja Keshar Kar *et al* 2022 *J. Phys.: Condens. Matter* **34** 075702

View the [article online](#) for updates and enhancements.

## You may also like

- [Antiferromagnetic coupling in Co/Ge superlattices](#)  
Yasushi Endo, N Kikuchi, O Kitakami *et al.*
- [Review of the thermoelectric properties of layered oxides and chalcogenides](#)  
A I Romanenko, G E Chebanova, Tingting Chen *et al.*
- [Ternary mixed magnetic Co/Mn/Ni dichloride dihydrate](#)  
G C DeFotis, A S Hampton and J M Pothen

# Effect of Co and Mg doping at Cu site on structural, magnetic and dielectric properties of $\alpha$ -Cu<sub>2</sub>V<sub>2</sub>O<sub>7</sub>

Abja Keshar Kar<sup>1</sup>, Bidisa Chattopadhyay<sup>1,\*</sup>, Ratnadwip Singha<sup>2,8</sup>,  
Abhisikta Barman<sup>3</sup>, Md A Ahmed<sup>4</sup>, A Midya<sup>5</sup>, S Bandyopadhyay<sup>6,7</sup>,  
Devajyoti Mukherjee<sup>3</sup>, D Jana<sup>6</sup> and Prabhat Mandal<sup>2</sup>

<sup>1</sup> Department of Physics, Lady Brabourne College, P-1/2 Suhrawardy Avenue, Kolkata 700 017, India

<sup>2</sup> Saha Institute of Nuclear Physics, HBNI, 1/AF Bidhannagar, Kolkata 700 064, India

<sup>3</sup> School of Physical Sciences, Indian Association for the Cultivation of Science, 2A and 2B Raja S. C. Mullick Road, Kolkata 700032, India

<sup>4</sup> Department of Physics, Sambhunath College, Labpur, Birbhum-731 303, West Bengal, India

<sup>5</sup> Department of Physics, City College, 102/1, Raja Rammohan Sarani, College Street, Kolkata 700 009, India

<sup>6</sup> Department of Physics, University of Calcutta, 92 A.P.C. Road, Kolkata 700 009, India

<sup>7</sup> CRNN, University of Calcutta, JD 2, Sector III, Salt Lake, Kolkata 700 098, India

E-mail: [bidisa\\_chattopadhyay@rediffmail.com](mailto:bidisa_chattopadhyay@rediffmail.com)

Received 6 September 2021, revised 7 November 2021

Accepted for publication 11 November 2021

Published 30 November 2021



## Abstract

We have studied the effect of doping of both magnetic (Co) and nonmagnetic (Mg) ions at the Cu site on phase transition in polycrystalline  $\alpha$ -Cu<sub>2</sub>V<sub>2</sub>O<sub>7</sub> through structural, magnetic, and electrical measurements. X-ray diffraction reveals that Mg doping triggers an onset of  $\alpha$ - to  $\beta$ -phase structural transition in Cu<sub>2-x</sub>Mg<sub>x</sub>V<sub>2</sub>O<sub>7</sub> above a critical Mg concentration  $x_c = 0.15$ , and both the phases coexist up to  $x = 0.25$ . Cu<sub>2</sub>V<sub>2</sub>O<sub>7</sub> possesses a non-centrosymmetric crystal structure and antiferromagnetic ordering along with a non-collinear spin structure in the  $\alpha$  phase, originated from the microscopic Dzyaloshinskii–Moriya interaction between the neighboring Cu spins. Accordingly, a weak ferromagnetic (FM) behavior has been observed up to  $x = 0.25$ . However, beyond this concentration, Cu<sub>2-x</sub>Mg<sub>x</sub>V<sub>2</sub>O<sub>7</sub> exhibits complex magnetic properties. A clear dielectric anomaly is observed in  $\alpha$ -Cu<sub>2-x</sub>Mg<sub>x</sub>V<sub>2</sub>O<sub>7</sub> around the magnetic transition temperature, which loses its prominence with the increase in Mg doping. The analysis of experimental data shows that the magnetoelectric coupling is nonlinear, which is in agreement with the Landau theory of continuous phase transitions. Co doping, on the other hand, initiates a sharp  $\alpha$  to  $\beta$  phase transition around the same critical concentration  $x_c = 0.15$  in Cu<sub>2-x</sub>Co<sub>x</sub>V<sub>2</sub>O<sub>7</sub> but the FM behavior is very weak and can be detected only up to  $x = 0.10$ . We have drawn the magnetic phase diagram which indicates that the rate of suppression in transition temperature is the same for both types of doping, magnetic (Co) and nonmagnetic (Zn/Mg).

Keywords: weak ferromagnetism, Dzyaloshinskii–Moriya interaction, structural phase transition, dielectric properties

(Some figures may appear in colour only in the online journal)

<sup>8</sup> Present address: Department of Chemistry, Princeton University, Princeton, New Jersey 08544, US

\* Author to whom any correspondence should be addressed.

## 1. Introduction

Magnetic materials with non-centrosymmetric (NCSM) crystal structure often exhibit novel phenomena induced by interacting spins. For example, the Dzyaloshinskii–Moriya (DM) interaction which is a microscopic characteristic of two interacting spins favors canting of spins and thereby introduces a non-collinear spin ordering such as helical or canted antiferromagnetic (AFM) order [1, 2]. Such a non-collinear spin structure induces ferroelectric (FE) polarization in some compounds, which are called magnetic ordering induced multiferroic materials. This phenomenon was first discovered by Kimura *et al* in hexagonal manganite  $\text{TbMnO}_3$  in which a special type of magnetic ordering stabilizes below 28 K and as a result, a non-zero electric polarization is observed [3]. Moreover, a polarization flop occurs under the action of external magnetic field along a certain crystallographic direction. Later on, a number of such materials have been discovered which attracted great attention due to their potential applications for functional devices such as magnetic sensors, multiple state memory devices, spintronic devices, and so on [4–6].

It is believed that the NCSM crystal structure and non-collinear magnetic structure bear an intimate relationship to establish multiferroicity via DM interaction in several metal–oxygen clusters [7–9]. However, a few more mechanisms have also been proposed in recent years to explain the magnetoelectric (ME) coupling in these materials. Aguilar *et al* studied magneto-infrared transmission in  $\text{TbMnO}_3$  and proposed a mechanism of ME dynamics involving only the isotropic Heisenberg exchange between non-collinear spins [10]. Using a theoretical model based on symmetric Heisenberg exchange, they clarified the origin of novel electromagnon excitations in cycloidal  $\text{RMnO}_3$ , although much weaker DM interaction was found to be the origin of static polarization. In some studies, an exchange–striction based mechanism, which generally occurs in non-polar crystals having collinear magnetic structure, is proposed [11]. Spin-dependent  $p$ – $d$  hybridization, which is of purely electronic origin, has also been discussed as a possible mechanism for ME coupling in Cu-based divanadates [12]. However, the acceptance of an appropriate mechanism is still in debate. To unveil the microscopic origin for the occurrence of multiferroicity in these materials, various investigations have been made following different routes [13–16]. Among them, chemical doping has been regarded as an effective tool to study the origin of ME coupling [17–22]. With these studies, one can explore the effect of doping on the intimate relationship between magnetic and crystal structures in these materials, which in turn, helps to gain insight into the stability of the microscopic interactions responsible for multiferroic ordering [23–25]. The effect of magnetic and nonmagnetic transition metal (TM) ion doping on the relative stability of the multiferroic phase of  $\text{Fe}_{1-x}\text{TM}_x\text{VO}_4$  has been studied [21]. This study offers the interesting possibility of using a large dopant fraction to tune the ME coupling in  $\text{FeVO}_4$ . Another study on the effect of doping of Cu and Co at the Ni site in  $\text{Ni}_3\text{V}_2\text{O}_8$  has shown that the

spin structure responsible for the development of FE ordering in this compound is relatively robust against perturbations produced by magnetic dopants and highlights the possibility of introducing new magnetic functionalities into multiferroics through magnetic ion doping [20]. Several studies have shown that better magnetic property can be achieved by increasing the Eu content at the Bi site in multiferroic  $\text{BiFeO}_3$  [18, 22].

Recently, pyrovanadates with the general formula  $M_2V_2O_7$  ( $M = \text{Cu, Ni, Co}$ ) have been revisited due to their diverse crystal structures and fascinating electric and magnetic properties [8, 26–28]. Copper-based pyrovanadate  $\alpha$ - $\text{Cu}_2\text{V}_2\text{O}_7$  has attracted great attention due to its magnetic ordering induced multiferroic properties [11, 29, 30]. Sanigrahi *et al*, have reported a spontaneous electric polarization of magnitude  $0.55 \mu\text{C cm}^{-2}$ , highest among the copper based improper multiferroic materials [11].  $\text{Cu}_2\text{V}_2\text{O}_7$  generally crystallizes in two stable polymorphs, low-temperature  $\alpha$ - and high-temperature  $\beta$ -phase, having phase transition temperature  $712^\circ\text{C}$ . The  $\alpha$ -phase is orthorhombic and NCSM with  $Fdd2$  symmetry whereas  $\beta$ -phase is monoclinic and centrosymmetric (CSM) with  $C2/c$  symmetry. Here, vanadium ion,  $\text{V}^{5+}$  ( $3d^0$ ), is non-magnetic and the total magnetic moment in this compound arises completely from  $\text{Cu}^{2+}$  ( $3d^9$ ) cations. In the  $\alpha$ -phase,  $\text{CuO}_5$  polyhedra are attached one another by edge-sharing and form a honeycomb-like spin structure with two mutually perpendicular spin chains which are separated by  $(\text{V}_2\text{O}_7)^{2-}$  anion groups consisting of corner-sharing  $\text{VO}_4$  tetrahedra (figure 1). The local coordination geometry of the Cu ion in the two phases determines their magnetic properties [8]. In figure 1, each Cu ion is coupled to its nearest neighbors (NN) by two asymmetric bonds  $\text{Cu-O}(1)\text{-Cu}$  and  $\text{Cu-O}(2)\text{-Cu}$ . In presence of a center of inversion located at the mid point of the line joining the two NN spins, DM vector becomes zero. But if an asymmetric bonding geometry exists in an AFM spin–lattice background, two non-compensating DM vectors appear which do not cancel each other, and hence induce a net DM interaction. Therefore, it favors canting of spins which induces a non-collinear spin ordering and an associated weak ferromagnetic (FM) moment. In  $\alpha$ - $\text{Cu}_2\text{V}_2\text{O}_7$ , exactly such situation arises. However, in the  $\beta$ -phase, the Cu ions are coupled via symmetric bonds and, thereby, the DM interaction is absent (figure 1). As a result, the magnetic structure of the  $\beta$ -phase is purely AFM [8, 9].  $\alpha$ - $\text{Cu}_2\text{V}_2\text{O}_7$  undergoes a transition to a long-range magnetic ordering state below  $\sim 33$  K with a canted AFM structure [8, 9, 11]. In this system, the appearance of a non-zero electric polarization with an associated weak FM ordering and their intimate coupling have also been demonstrated in some recent works [9, 11, 12, 26].

Another divanadate,  $\text{Co}_2\text{V}_2\text{O}_7$ , crystallizes in a monoclinic structure with  $P2_1/c$  symmetry [26, 31]. Recent studies have reported two fascinating magnetization plateaus—a  $1/2$  like and a  $3/4$  plateau depending on the crystallographic directions [27, 32]. Magnetic field-induced ferroelectricity correlated with the magnetization plateaus was also observed in this system [27]. Furthermore, neutron powder diffraction and magnetization data have confirmed a non-collinear magnetic

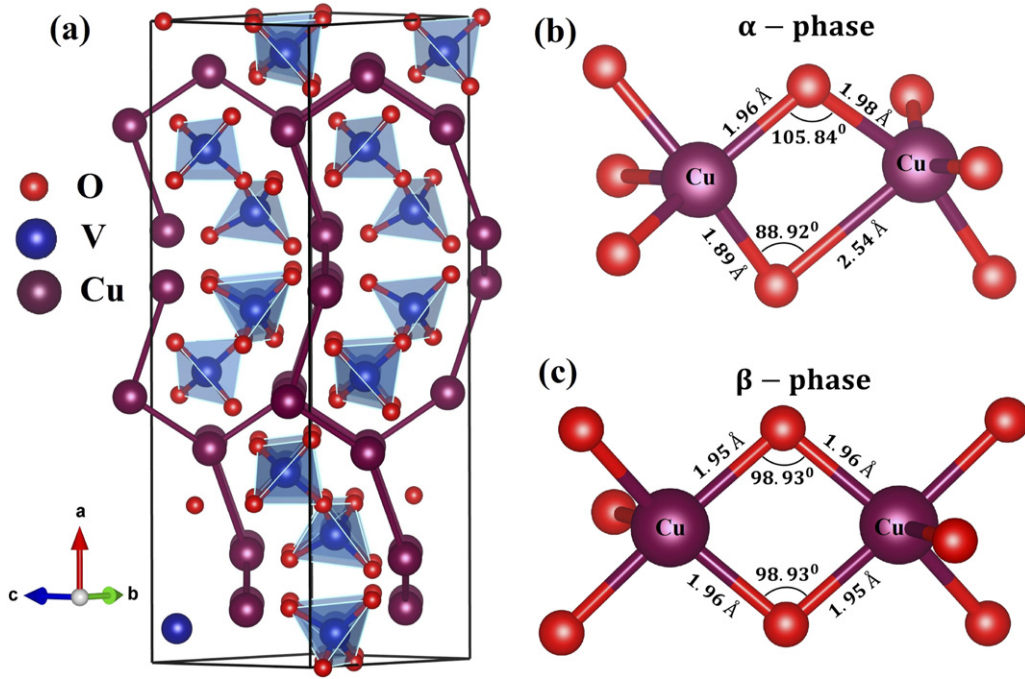


**Figure 1.** (a) Crystal structure of  $\alpha$ - $\text{Cu}_2\text{V}_2\text{O}_7$  showing honeycomb like  $\text{Cu}^{2+}$  spin configuration with two mutually perpendicular spin chains which are separated by  $(\text{V}_2\text{O}_7)^{2+}$  anion groups consisting of corner-sharing  $\text{VO}_4$  tetrahedra. (b) Nearest neighbor Cu atoms connected by two asymmetric bonds  $\text{Cu}-\text{O}(1)-\text{Cu}$  and  $\text{Cu}-\text{O}(2)-\text{Cu}$  in the  $\alpha$ -phase. (c) Symmetric  $\text{Cu}-\text{O}$  bonds for connecting NN Cu atoms in the  $\beta$ -phase.

structure with canted  $\uparrow\uparrow\downarrow\downarrow$  spin configuration as the origin of ME coupling [28].

Till date, to the best of our knowledge, very few studies on pyrovanadate  $\text{Mg}_2\text{V}_2\text{O}_7$  have been conducted. Recently, Tena *et al* have reported that evolution of  $\alpha$ - or  $\beta$ -phase in  $\text{Cu}_{2-x}\text{Mg}_x\text{V}_2\text{O}_7$  depends on the synthesis temperature [33]. When prepared at  $600^\circ\text{C}$ , only crystalline phase with  $\alpha$ - $\text{Cu}_2\text{V}_2\text{O}_7$  structure is present for  $x < 0.5$  and  $\beta$ - $\text{Cu}_2\text{V}_2\text{O}_7$  structure evolves for  $x \geq 0.5$ . On the other hand, Zn doping in  $\alpha$ - $\text{Cu}_{2-x}\text{Zn}_x\text{V}_2\text{O}_7$  triggers  $\alpha$ - to  $\beta$ -phase transition beyond a critical Zn concentration  $x_c = 0.15$  [8, 9]. It has also been confirmed that the ME coupling exists only in  $\alpha$ - $\text{Cu}_2\text{V}_2\text{O}_7$  but not in  $\beta$ -phase [9]. So, like spin-zero Zn, Mg may also establish itself as an interesting candidate to perform the doping dependent studies in Cu-divanadate system.

In this paper, we report the magnetic and electrical properties of  $\text{Cu}_{2-x}\text{M}_x\text{V}_2\text{O}_7$  ( $M = \text{Co}, \text{Mg}$ ) through structural, magnetization, heat capacity, and dielectric measurements. The main aim of our work is to study the robustness of magnetic phase transition and ME properties against magnetic (Co) and non-magnetic (Mg) doping at Cu site. An onset of phase transition from the NCSM ( $\alpha$ ) to a CSM ( $\beta$ ) phase has been observed through Mg as well as Co doping around the same critical concentration  $x_c = 0.15$  as in the case of  $\text{Cu}_{2-x}\text{Zn}_x\text{V}_2\text{O}_7$  system. In the Mg-doped system, a significant magnetodielectric effect has been observed only in the  $\alpha$ -phase but not in its  $\beta$ -phase. Finally, we have constructed a magnetic phase diagram for  $\text{Cu}_{2-x}\text{M}_x\text{V}_2\text{O}_7$  by plotting the magnetic transition temperature vs doping concentration. We believe that this study will help

to identify the ME behavior against small perturbations in the magnetic network of Cu-based divanadates.

## 2. Experimental technique and sample preparation

We have prepared polycrystalline  $\text{Cu}_{2-x}\text{Mg}_x\text{V}_2\text{O}_7$  samples with compositions  $x = 0, 0.10, 0.15, 0.20, 0.25, 0.30$  and  $0.40$  and  $\text{Cu}_{2-x}\text{Co}_x\text{V}_2\text{O}_7$  with  $x = 0, 0.05, 0.10, 0.15, 0.20$  and  $2.0$  by standard solid-state reaction technique. Appropriate amounts of  $\text{CuO}$ ,  $\text{MgO}$ ,  $\text{CoO}$ , and  $\text{V}_2\text{O}_5$  powders were mixed to obtain the desired composition. The precursors were dissolved in ethanol for homogeneous mixing and then heated in air at  $600^\circ\text{C}$  for 100–150 h with several intermediate grindings. The resulting powder was then pressed into pellets using polyvinyl alcohol as the binder and finally sintered at  $600^\circ\text{C}$  for 10 h. We have investigated the structure of these samples using x-ray diffraction measurement with a Rigaku TTRAX III diffractometer having  $\text{Cu}-\text{K}\alpha$  radiation in the  $2\theta$  range from  $10^\circ$  to  $80^\circ$ . The magnetization was measured up to a maximum field of 20 kOe in a superconducting quantum interference device-vibrating sample magnetometer (MPMS 3, quantum design). Heat capacity measurements were performed in absence of applied magnetic field in a physical property measurement system (quantum design). A cryostat (Cryogenic Ltd.) operating over a temperature range of 2–300 K was used to carry out the dielectric measurements in a two-probe set-up using conducting silver paste and gold wire. In this measurement, we have used an Andeen-Hagerling ultra-precision

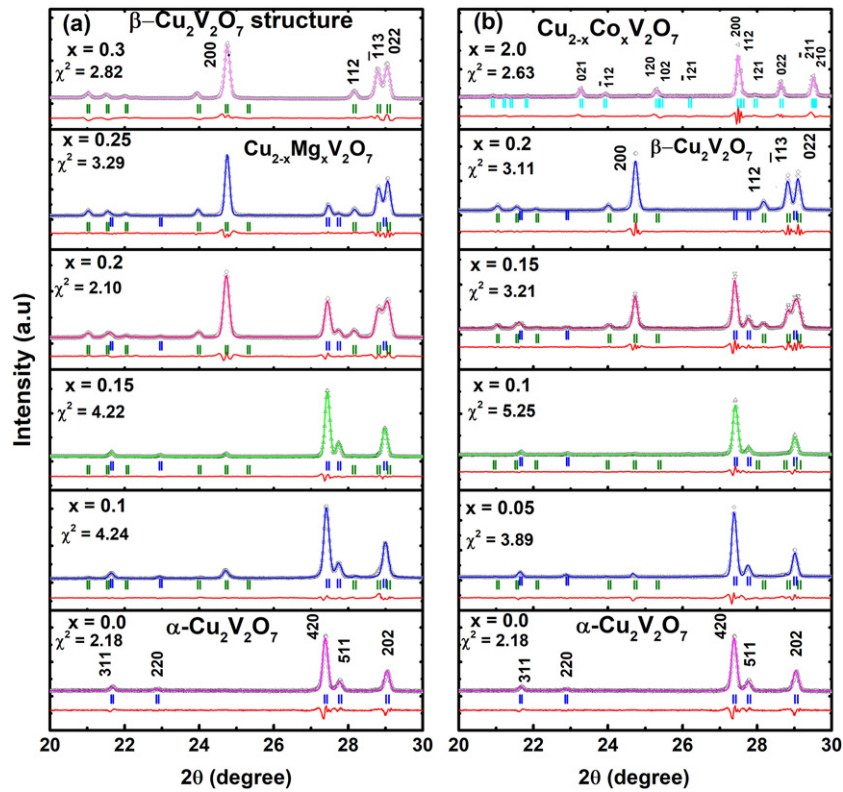


**Figure 2.** Refined x-ray diffraction patterns for (a)  $\text{Cu}_{2-x}\text{Mg}_x\text{V}_2\text{O}_7$  and (b)  $\text{Cu}_{2-x}\text{Co}_x\text{V}_2\text{O}_7$  samples for  $2\theta$  in the range  $20^\circ$ – $30^\circ$ . The red lines represent the difference between the observed intensity and the calculated intensity. Vertical lines represent the Bragg positions for  $\alpha$ -phase (blue) and  $\beta$ -phase (olive) of  $\text{Cu}_{2-x}(\text{Mg}/\text{Co})_x\text{V}_2\text{O}_7$ . The vertical lines with cyan color represent the Bragg positions for  $\text{Co}_2\text{V}_2\text{O}_7$ . The parameters for the best fit results are shown in table 1.

capacitance bridge (Model AH2700A) in the frequency range 1–20 kHz.

### 3. Experimental results and discussions

#### 3.1. Structural Properties.

Refined x-ray diffraction patterns for  $\text{Cu}_{2-x}\text{M}_x\text{V}_2\text{O}_7$  ( $M = \text{Co}, \text{Mg}$ ) are shown in figures 2(a) and (b). X-ray diffraction patterns are shown over a limited interval of angle, where the  $\alpha$ - to  $\beta$ -phase transition can be seen clearly. We have shifted the curves along y-axis for clarity. Detailed Rietveld structural analysis results for the doped samples are presented in table 1. For a useful comparison, we have also included the corresponding data for  $\text{Cu}_{2-x}\text{Zn}_x\text{V}_2\text{O}_7$  from our earlier studies [9]. As shown in table 1,  $\text{Cu}_{2-x}\text{Mg}_x\text{V}_2\text{O}_7$  possess as much as 94%  $\alpha$ -phase for  $x = 0.15$ . However, the fraction of  $\alpha$ -phase drops abruptly to  $\sim 26\%$  as  $x$  increases from 0.15 to 0.20 only. Finally, for  $x = 0.30$ , an almost complete phase transition from  $\alpha$ - to  $\beta$ -phase is observed. A similar result has also been obtained in a recent study on  $\text{Cu}_{2-x}\text{Mg}_x\text{V}_2\text{O}_7$ , where the presence of 12.4% of  $\alpha$ -phase and 87.6% of  $\beta$ -phase have been reported for  $x = 0.25$ , in good agreement with our refinement result [33].  $\text{Cu}_{2-x}\text{Zn}_x\text{V}_2\text{O}_7$ , on the other hand, shows a clear  $\alpha$ - to  $\beta$ -phase transition around a critical Zn concentration,  $x_c = 0.15$ , as reported in our earlier work [9]. For  $x = 0.20$ , it shows a residue of only 2.7%  $\alpha$ -phase (table 1). So, x-ray structural analysis of Mg-doped  $\alpha$ - $\text{Cu}_2\text{V}_2\text{O}_7$  indicates an onset of

$\alpha$ - to  $\beta$ -phase transition around the same  $x_c = 0.15$  as in Zn-doped one. However, the transition for  $\text{Cu}_{2-x}\text{Mg}_x\text{V}_2\text{O}_7$  is not as sharp as in the case of Zn doping due to the coexistence of both the phases up to  $x = 0.25$ .  $\text{Cu}^{2+}$ ,  $\text{Zn}^{2+}$  and  $\text{Mg}^{2+}$  possess comparable ionic radii, 73, 74 and 72 pm, respectively [34]. The reason behind this difference in the behavior of  $\text{Zn}^{2+}$  and  $\text{Mg}^{2+}$  around the phase transition point is not clear.

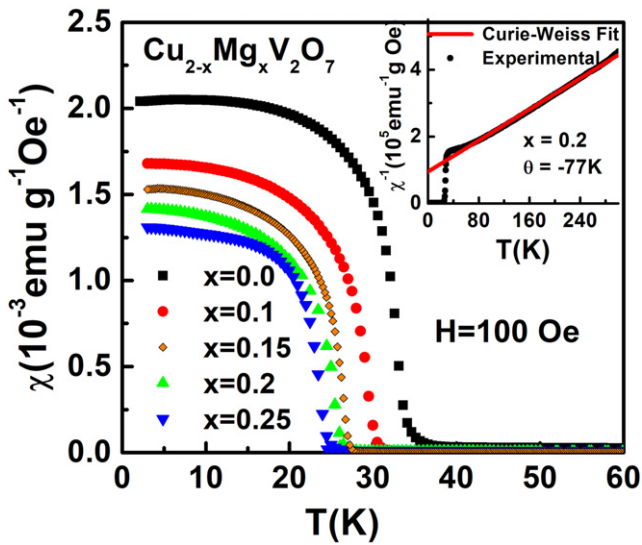
In contrast,  $\text{Co}^{2+}$  is a spin-3/2 magnetic ion and the end member  $\text{Co}_2\text{V}_2\text{O}_7$  is not isostructural to  $\beta$ - $\text{Cu}_2\text{V}_2\text{O}_7$ . Nevertheless, as shown in figure 2(b), Co doping also triggers a sharp  $\alpha$ - to  $\beta$ -structural phase transition around the same  $x_c = 0.15$ , as observed in  $\text{Cu}_{2-x}\text{Zn}_x\text{V}_2\text{O}_7$ . So, the phase transition point,  $x_c = 0.15$ , in Cu-based divanadate  $\alpha$ - $\text{Cu}_2\text{V}_2\text{O}_7$  appears to be independent of the type of dopant, i.e., whether it is magnetic or nonmagnetic. It is to be noted here that the ionic radius of  $\text{Co}^{2+}$  in high-spin configuration is 74.5 pm, which is slightly higher than 73 pm for  $\text{Cu}^{2+}$  [34]. So, the structural phase transition in  $\alpha$ - $\text{Cu}_2\text{V}_2\text{O}_7$  may not be an outcome of solely ionic size-dependent dopant effect. More such doping studies are necessary to resolve this issue.

#### 3.2. Magnetic properties

For  $\text{Cu}_{2-x}\text{M}_x\text{V}_2\text{O}_7$  ( $M = \text{Co}, \text{Mg}$ ), magnetic measurements are performed to identify the onset of magnetic correlations and to study the evolution of magnetic properties with doping. The dc magnetic susceptibility  $\chi$  for  $\text{Cu}_{2-x}\text{Mg}_x\text{V}_2\text{O}_7$  as a function of temperature from 3 to 50 K is plotted in figure 3 up

**Table 1.** Refined lattice parameters ( $a$ ,  $b$ ,  $c$ ), molar percent of  $\alpha$ - and  $\beta$ -phase in  $\text{Cu}_{2-x}\text{Mg}_x\text{V}_2\text{O}_7$  ( $M = \text{Mg}$ ,  $\text{Co}$  and  $\text{Zn}$ ) along with other characterizing parameters. The numbers in parenthesis are the error bar.

$x$	% of $\alpha$ phase ( $Fdd2$ )	% of $\beta$ phase ( $C2/c$ )	$\chi^2$	$T_N$ (K)	$\theta$ (K)	$a(\text{\AA})$	$b(\text{\AA})$	$c(\text{\AA})$
0.0(Cu)	100.0(0.6)	0.0	2.18	32.8(0.2)	-82.9	( $\alpha$ -)20.6532(0)	8.3930(0)	6.4414(0)
0.05(Co)	96.6(0.3)	3.4(0.3)	3.89	30.3(0.2)	-59.9	( $\alpha$ -)20.6513(4)	8.3833(1)	6.4440(1)
						( $\beta$ -)7.6846(0)	8.0614(0)	10.1179(0)
0.1(Zn)	95.1(0.9)	4.9(0.1)	1.25	28.9(0.1)	-89.4	( $\alpha$ -)20.6617(0)	8.3670(0)	6.4533(0)
						( $\beta$ -)7.6706(0)	8.0583(0)	10.1282(0)
0.1(Mg)	96.8(0.8)	3.2(0.7)	4.24	29.3(0.3)	-70	( $\alpha$ -)20.6799(2)	8.3704(1)	6.4505(1)
						( $\beta$ -)7.6848(9)	8.0956(0)	10.0709(11)
0.1(Co)	94.0(0.6)	6.0(0.6)	5.25	29.5(0.3)	-58.3	( $\alpha$ -)20.6453(0)	8.3779(0)	6.4479(0)
						( $\beta$ -)7.6679(0)	8.0544(0)	10.1526(0)
0.15(Zn)	93.0(0.9)	7.0(0.1)	1.21	26.6(0.2)	-50.7	( $\alpha$ -)20.6560(0)	8.3739(0)	6.4510(0)
						( $\beta$ -)7.6657(0)	8.0711(0)	10.1050(0)
0.15(Mg)	93.7(0.2)	6.3(0.0)	4.22	26.5(0.2)	-88.9	( $\alpha$ -)20.6874(0)	8.3564(0)	6.4532(0)
						( $\beta$ -)7.6817(0)	8.0548(0)	10.1214(0)
0.15(Co)	46.3(0.2)	53.7(0.1)	3.21	—	—	( $\alpha$ -)20.6530(0)	8.3820(0)	6.4486(0)
						( $\beta$ -)7.6808(0)	8.0448(0)	10.1107(0)
0.2(Zn)	2.7(0.5)	97.3(0.5)	1.15	25.4(0.1)	-70.7	( $\alpha$ -)20.6847(7)	8.3731(5)	6.4449(2)
						( $\beta$ -)7.6787(3)	8.0622(3)	10.1182(6)
0.2(Mg)	26.2(0.3)	73.8(0.2)	2.10	25.3(0.3)	-77	( $\alpha$ -)20.6986(0)	8.3518(0)	6.4566(0)
						( $\beta$ -)7.6810(0)	8.0628(0)	10.1160(0)
0.2(Co)	3.5(0.0)	96.5(0.4)	3.11	—	—	( $\alpha$ -)20.2671(0)	8.1920(0)	6.0731(0)
						( $\beta$ -)7.6785(0)	8.0536(0)	10.1108(0)
0.25(Mg)	10.2(0.2)	89.8(0.2)	3.29	23.5(0.3)	-54	( $\alpha$ -)20.6968(0)	8.3365(0)	6.4613(0)
						( $\beta$ -)7.6733(0)	8.0686(0)	10.1112(0)
0.3(Mg)	0.2(0.1)	99.8(0.1)	2.82	21.5(0.1)	—	( $\beta$ -)7.6752(1)	8.0752(1)	10.1177(1)

**Figure 3.** Static magnetic susceptibility ( $\chi$ ) as a function of temperature ( $T$ ) for  $\text{Cu}_{2-x}\text{Mg}_x\text{V}_2\text{O}_7$ . Inset shows  $\chi^{-1}$  vs  $T$  plot for  $x = 0.2$  and the corresponding Curie–Weiss fit (solid line).

to Mg concentration  $x = 0.25$  along with the undoped one in a magnetic field  $H = 100$  Oe. For all concentrations,  $\chi(T)$  shows a steep upturn around the Neel temperature  $T_N$ , indicating a transition to a magnetically ordered state with the lowering of temperature. We have fitted the high-temperature susceptibility data to Curie–Weiss expression ( $\chi = \frac{C}{T-\theta}$ ) for determining the important physical parameters such as the Curie–Weiss

temperature ( $\theta$ ) and Curie constant ( $C = \frac{Ng^2\mu_B^2J(J+1)}{3k_B}$ ), which describe the nature of the magnetic ground state of the system. A representative plot of the inverse magnetic susceptibility ( $\chi^{-1}$ ) against temperature for the  $x = 0.2$  sample is shown in the inset of figure 3. For all the samples,  $\theta$  (summarized in table 1) is found to be negative, indicating that the dominant exchange interaction is AFM in nature. The influence of negative  $\theta$  is clearly reflected in the  $\chi(T)$  behavior of the corresponding samples. As  $\theta$  signifies the effective average magnetic exchange, it decreases gradually due to the dilution of spins with increasing non-magnetic Mg concentration. Our experimental finding is in line with the prediction of density functional theory (DFT) for this system [11, 35, 36]. The results of DFT calculations suggest that AFM exchange interaction dominates magnetism. We have calculated the effective magnetic moment ( $\mu_{\text{eff}}$ ) from the value of  $C$ . With increase in  $x$ ,  $\mu_{\text{eff}}$  gradually decreases from  $2.09 \mu_B/\text{Cu}$  ion for  $x = 0$  to  $0.9 \mu_B/\text{Cu}$  ion for  $x = 0.25$ . This result is expected because the higher spin  $\text{Cu}^{2+}$  ( $S = \frac{1}{2}$ ) is being removed from the lattice and replaced with increasing fractions of  $\text{Mg}^{2+}$  with  $S = 0$ . The effective magnetic moment  $2.09 \mu_B/\text{Cu}$  ion for the undoped  $\text{Cu}_2\text{V}_2\text{O}_7$  is slightly larger than the spin only value  $\mu_{\text{eff}} = g\mu_B\sqrt{S(S+1)} = 1.73 \mu_B$  ( $g = 2$  and  $S = \frac{1}{2}$  per  $\text{Cu}^{2+}$  ion) which may be due to some amount of mixing of the orbital moment, characteristic of the  $\text{Cu}^{2+}$  cation [9]. As  $\text{Cu}^{2+}$  is in a  $3d^9$  electronic configuration, the spin–orbit interaction is not completely ignorable. Here, the spin–orbit interaction comes in as a perturbation, and as a result, we expect a small contribution of orbital degrees of freedom to the total moment. This results in a quenched ground state, but with a  $\mu_{\text{eff}}$  slightly

larger (of the order of a few tenths of a Bohr Magnetron) than the spin only value [37, 38].

$T_N$  also gradually decreases with  $x$ , from 32.8 K for  $x = 0$  to 23.5 K for  $x = 0.25$  which is expected as Mg doping increases the average distance between neighboring Cu spins, resulting in a decrease of effective average magnetic exchange. The presence of weak FM ordering in  $\text{Cu}_{2-x}\text{Mg}_x\text{V}_2\text{O}_7$  for  $x \leq 0.25$  can be attributed to the coexistence of  $\alpha$ - and  $\beta$ -phase up to this concentration (table 1). However, such FM ordering in  $\text{Cu}_{2-x}\text{Zn}_x\text{V}_2\text{O}_7$  suppresses completely for compositions above  $x_c = 0.15$  due to the absence of  $\alpha$ -phase above this critical concentration [8, 9]. Thus magnetic studies also confirm that nonmagnetic Mg and Zn doping behave slightly differently around the phase transition point in  $\alpha$ - $\text{Cu}_{2-x}\text{M}_x\text{V}_2\text{O}_7$ . We have estimated the Heisenberg intrachain exchange interaction  $J$  using the relation  $\theta = \frac{-2ZJ(S(S+1))}{3k_B}$  in mean-field approximation [8] and considering the number of NN as  $Z = 2$ .  $J$  is found to be  $\sim 80$  and  $\sim 70$  K for  $x = 0$  and  $x = 0.10$ , respectively. Such a significantly low value of  $J$  compared to  $J \sim 1500$  K for two-dimensional cuprates having  $180^\circ$  Cu–O–Cu bonds indicates not much deviation of the Cu–O–Cu bonds from  $90^\circ$ , in agreement with Goodenough–Kanamori–Anderson rules [8].

Figure 4 shows temperature dependence of dc magnetic susceptibility  $\chi$  for  $\text{Cu}_{2-x}\text{Mg}_x\text{V}_2\text{O}_7$  with  $x = 0.30$  and  $0.40$ . A drastic change in the behavior of  $\chi(T)$  for  $x = 0.30$  has been observed, as shown in figure 4(a). Instead of a steep upturn,  $\chi(T)$  shows a broad maximum at  $T_{\text{max}} = 38.5$  K (comparable to  $T_{\text{max}} = 36$  K for  $x = 0.30$  in  $\text{Cu}_{2-x}\text{Zn}_x\text{V}_2\text{O}_7$  [9]), indicating the signature of a one-dimensional Heisenberg AFM spin chain [39]. At low-temperature below 8.5 K, the upturn in  $\chi(T)$  may be attributed to a Curie-like tail due to the presence of isolated spins at the defect sites, which is quite common in such a low-dimensional system [40, 41]. However, no clear evidence of magnetic ordering has been detected, possibly due to the sharp fall of  $\chi(T)$  slightly below  $T_{\text{max}}$ . For this reason, we have performed heat capacity measurement (to be discussed in detail in a later section) for this sample, and a  $\lambda$ -like anomaly is observed around  $T_N = 21.5$  K due to long-range AFM ordering (figure 9(a)). We have then looked into the next higher concentration sample  $x = 0.40$ . Similar to  $x = 0.30$  sample,  $\chi(T)$  for  $x = 0.40$  shows a broad maximum at  $T_{\text{max}} = 30$  K with an additional cusp around 19 K (figure 4(b)), indicating a clear transition to a magnetically ordered state at low temperature. In order to understand the nature of the magnetic state of these samples, the  $\chi(T)$  data have been fitted with the well-known Bonner–Fisher (BF) model, considering it as a 1D AFM spin-chain system [39]. For such a low-dimensional system, the magnetic susceptibility is often expressed as a sum of three contributions,

$$\chi(T) = \chi_o + \chi_{\text{BF}}(T) + \chi_{\text{defect}}(T), \quad (1)$$

where the temperature-independent term  $\chi_o$  is the sum of the diamagnetic susceptibility of the doped sample and the Van-Vleck paramagnetism of  $\text{Cu}^{2+}$  cation and  $\chi_{\text{defect}}(T)$  is the Curie–Weiss susceptibility of the defect magnetic sites contributing to the low-temperature upturn in  $\chi(T)$  whereas  $\chi_{\text{BF}}(T)$  is the BF susceptibility arising from the spin–spin

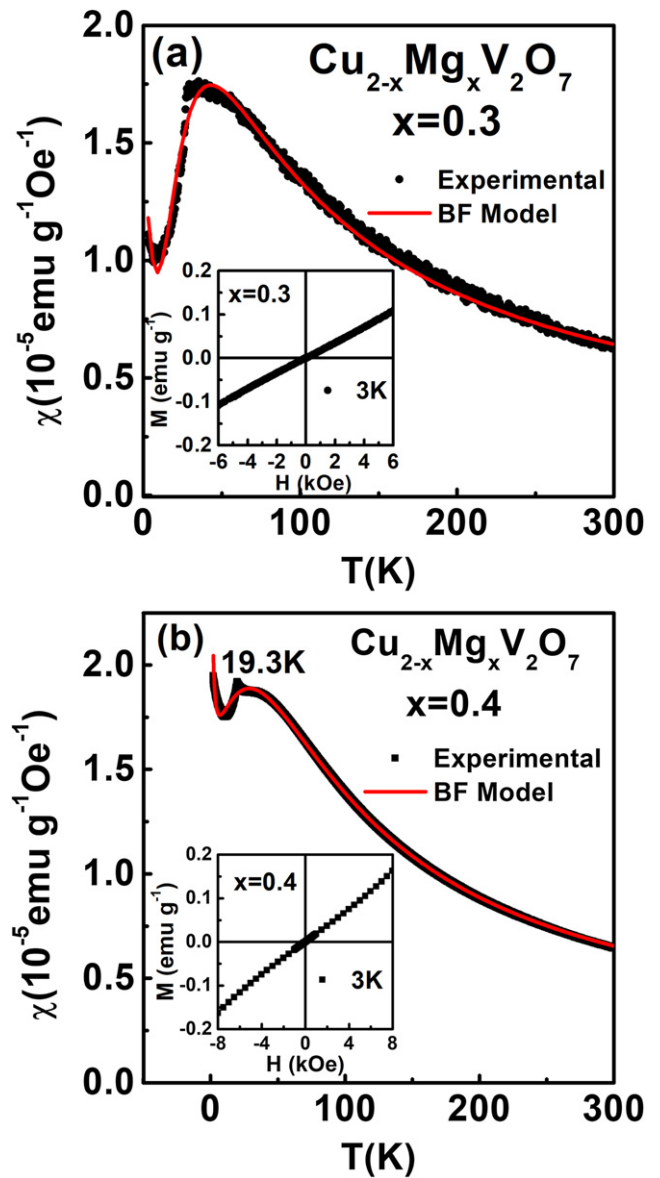


**Figure 4.** Temperature dependence of static magnetic susceptibility  $\chi$  of  $\text{Cu}_{2-x}\text{Mg}_x\text{V}_2\text{O}_7$  for  $x = 0.30$  (a) and  $0.40$  (b). Solid line is a fit to the experimental data following BF model. Lower insets of (a) and (b): field dependence of magnetization  $M(H)$  of  $\text{Cu}_{2-x}\text{Mg}_x\text{V}_2\text{O}_7$  for  $x = 0.30$  and  $0.40$ , respectively below  $T_N$  showing no hysteresis.

correlation. Solid lines shown in figure 4 represent the fit to the experimental data following the BF model assuming  $g = 2.13$  found from electron paramagnetic resonance measurements for similar concentration of Zn-doped  $\text{Cu}_{2-x}\text{Zn}_x\text{V}_2\text{O}_7$  [8]. From the fitted parameters,  $J$  is found to be 30 and 20 K for  $x = 0.30$  and  $0.40$ , respectively. Nevertheless, the height and the position of the maximum of  $\chi(T)$  are reproduced well for these samples.

In this context, we would like to mention that the  $\chi(T)$  curve for  $\beta$ - $\text{Cu}_2\text{V}_2\text{O}_7$  also exhibits a broad peak. Several groups attributed this broad peak to the short-range ordering of 1D AFM spin chain [8, 41, 42]. Both He *et al* and Pommer *et al* analyzed the temperature dependence of susceptibility using the BF model [8, 41]. Touaiher *et al* also fitted the  $\chi(T)$  curve

with 1D spin-chain but they concluded spin-singlet ground state, i.e., formation of spin-dimer at low temperature [42]. However, Tsirlin *et al* analyzed the susceptibility data using a two-dimensional (2D) AFM model and claim that their fit is slightly better than that with the 1D BF spin-chain model [43]. Recently, high-frequency electron spin resonance (ESR) measurements were carried out on single crystal of  $\beta$ - $\text{Cu}_2\text{V}_2\text{O}_7$  down to 4.2 K to shed some light on this issue [44]. ESR data suggest that 1D alternating-chain model is the most reasonable candidate for explaining the magnetic properties of the crystal. We believe that neutron scattering and other microscopic techniques on high-quality single crystals may help to resolve this issue.

For  $x = 0.30$  and  $0.40$ ,  $J$  can also be estimated from the position of the maximum of the  $\chi(T)$  curve, using the relation  $T_{\text{max}} = \frac{1.282J}{k_B}$  for 1D AFM spin-chain system [45].  $J$  is found to be 30 and 23 K for  $x = 0.30$  and  $0.40$ , respectively, in agreement with the corresponding values 30 and 20 K calculated using the BF model. Another very important parameter related to AFM spin chain is the inter-chain coupling ( $J_{\text{inter}}$ ) strength. Inter-chain coupling can be estimated using the relation  $2J_{\text{inter}} = \frac{T_N}{1.28\sqrt{\ln(\frac{3.8J}{T_N})}}$  in the mean-field approximation [8].

Considering  $J = 30$  and  $23$  K and corresponding  $T_N$  as 21.5 and 19.3 K for  $x = 0.30$  and  $0.40$ , respectively, the values of  $J_{\text{inter}}$  are found to be  $\sim 6$  K and 5 K. So, we infer that the presence of a significant inter-chain coupling  $J_{\text{inter}}$  along with intra-chain interaction  $J$  in  $\text{CuO}_5$  complexes may drive the system into a magnetically ordered state at low temperature. The ratio of  $J_{\text{inter}}$  to  $J$  as estimated for  $x = 0.30$  and  $0.40$  samples is  $\sim 0.2$ . This ratio estimated by different other groups based on experimental studies is found to be  $\sim 0.354$  in single crystal of  $\beta$ - $\text{Cu}_2\text{V}_2\text{O}_7$  [41] and  $\sim 0.17$  in Zn-doped  $\text{Cu}_2\text{V}_2\text{O}_7$  with  $x = 0.30$  [8]. Tsirlin *et al* found this ratio to be  $\sim 0.2$  in  $\beta$ - $\text{Cu}_2\text{V}_2\text{O}_7$ , based on the theoretical calculations considering a spin- $\frac{1}{2}$  anisotropic honeycomb lattice model [43]. These values are much larger than that for  $\text{LiCuVO}_4$  ( $\sim 0.045$ ) [46] and  $\text{BaCu}_2\text{Si}_2\text{O}_7$  ( $\sim 0.011$ ) [47] which are well known quasi-1D spin-chain systems and undergo a three-dimensional magnetic ordering at low temperature. Thus Cu-divanadate shows a less pronounced 1D character.

We have also measured the field dependence of magnetization  $M$  for  $\text{Cu}_{2-x}\text{Mg}_x\text{V}_2\text{O}_7$  both above and below the Neel temperature  $T_N$ . One representative plot for each composition  $x = 0.25$  and  $0.10$  is shown in figure 5. All the samples up to  $x = 0.25$  show a clear hysteresis below  $T_N$  but  $M(H)$  exhibits a linear behavior well above  $T_N$  up to the highest measured magnetic field 5 kOe. On the other hand,  $x = 0.30$  and  $0.40$  samples do not show any hysteresis below  $T_N$  (insets of figures 4(a) and (b)). The above results are in good agreement with the corresponding  $M(T)$  data, confirming the existence of weak ferromagnetism in  $\text{Cu}_{2-x}\text{Mg}_x\text{V}_2\text{O}_7$  up to  $x = 0.25$ . The high-field linear behavior of  $M(H)$  curve can be fitted with the empirical relation  $M(H) = \chi_{\text{AFM}}H + M(0)$  (figure 5). From the fitted parameters, we obtain the saturation magnetization  $M(0)$ , i.e., the canted moment at zero field as intercept whereas the linear term gives the AFM component.  $M(0)$  for all the samples up to  $x_c = 0.15$  is found to be  $\sim 0.03 \mu_B/\text{Cu-ion}$ , including

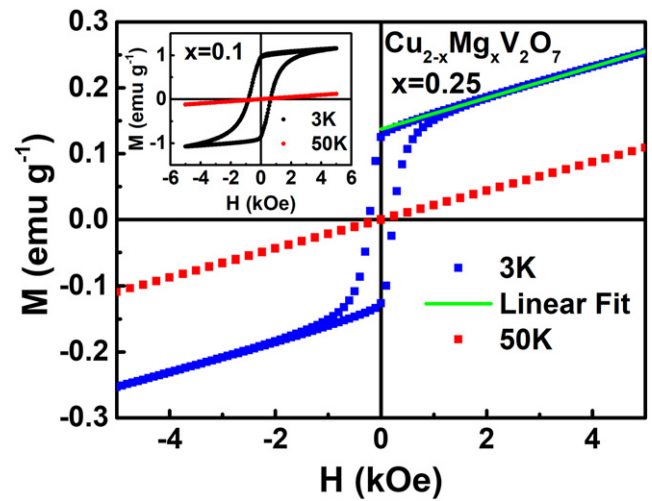


**Figure 5.** Field dependence of magnetization of  $\text{Cu}_{2-x}\text{Mg}_x\text{V}_2\text{O}_7$  for  $x = 0.25$  below (3 K) and above (50 K)  $T_N$  along with the linear fitting of the high field data. Inset shows  $M(H)$  data below and above  $T_N$  for  $x = 0.10$ .

the undoped  $\alpha$ - $\text{Cu}_2\text{V}_2\text{O}_7$ , in agreement with Zn-doped system [8, 9]. The full saturation moment of a single  $\text{Cu}^{2+}$  ion is one  $\mu_B$  which is much larger than the above-mentioned value of the canted moment. Canting angle ( $\phi_{\text{DM}}$ ), which can be determined through the relation  $\tan \phi_{\text{DM}} = \frac{M(0)}{8\mu_B S}$ , is found to be  $\sim 2^\circ$ , same for all Mg-doped samples up to  $x_c = 0.15$ . On the other hand, beyond  $x_c = 0.15$ , canting angle gradually decreases to  $0.66^\circ$  and  $0.24^\circ$  for  $x = 0.20$  and  $x = 0.25$ , respectively. The above analysis indicates that in the  $\alpha$ -phase, nonmagnetic Mg doping does not change the nature of the exchange interaction, though it weakens the AFM exchange coupling between the neighboring Cu spins due to which  $T_N$  gradually decreases. Above  $x_c = 0.15$ ,  $\beta$ -phase starts to dominate [see table 1] and hence  $M(0)$  and the canting angle gradually decrease.

The temperature dependence of magnetic susceptibility for  $\text{Cu}_{2-x}\text{Co}_x\text{V}_2\text{O}_7$  ( $x = 0, 0.05, 0.10$  and  $2.0$ ) in an applied field of 500 Oe is shown in figures 6 and 7. A sharp rise in  $\chi(T)$  below  $T_N$  and thereby, a saturation, indicating a transition to a magnetically ordered state persists up to  $x = 0.05$ . From the Curie-Weiss fit,  $\theta$  and  $\mu_{\text{eff}}$  are found to be  $-59.9$  K and  $1.95 \mu_B$ , respectively for  $x = 0.05$ , indicating a decrease in  $\theta$  with respect to undoped  $\alpha$ - $\text{Cu}_2\text{V}_2\text{O}_7$  ( $\theta = -82.9$  K). For this concentration, below  $\sim 27$  K, a clear bifurcation is observed between the field-cooled heating (FCH) and zero-field-cooled heating (ZFCH) curve with a coercive field of 544 Oe in the corresponding  $M(H)$  data (figure 6). The observed results suggest the presence of some kind of magnetic frustration due to the coexistence of FM and AFM phases. For  $x = 0.10$ ,  $\chi(T)$  shows a kink around 29 K, indicating an onset of spin-spin correlation for a low-dimensional magnet and thereby, again increases and finally shows a slight tendency of saturation specifying a transition to a magnetically ordered state. Here also, a small bifurcation between FCH and ZFCH curves is observed at low temperature, indicating the presence of a residual FM phase. This observation can be verified from the corresponding  $M(H)$  curve (figure 8). At  $T = 2$  K,

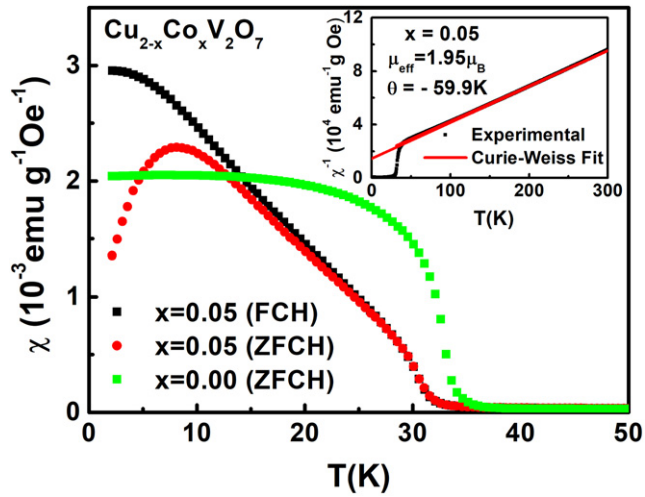


**Figure 6.** Temperature dependence of static magnetic susceptibility  $\chi$  of  $\text{Cu}_{2-x}\text{Co}_x\text{V}_2\text{O}_7$  for an applied magnetic field  $H = 500$  Oe for  $x = 0.05$  and  $H = 100$  Oe for  $x = 0$ . Inset shows  $\chi^{-1}(T)$  for  $x = 0.05$  with a fit to the Curie–Weiss law (solid line).

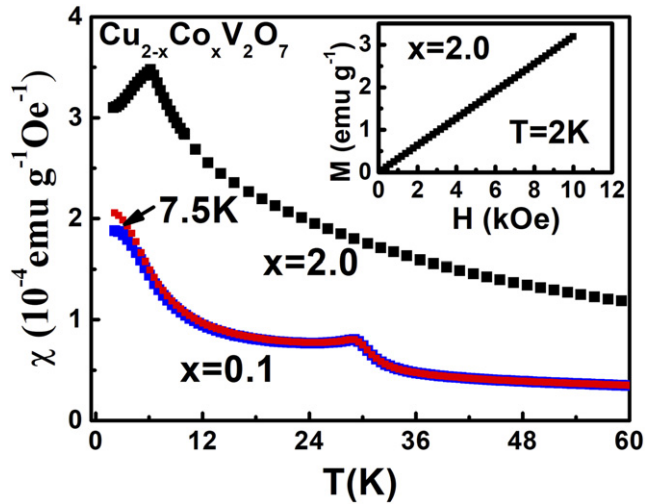


**Figure 7.** Temperature dependence of static magnetic susceptibility  $\chi$  of  $\text{Cu}_{2-x}\text{Co}_x\text{V}_2\text{O}_7$  for  $x = 0.10$  and  $x = 2.0$  for an applied magnetic field  $H = 500$  Oe. Inset shows field dependence of magnetization  $M$  in the first quadrant for  $x = 2.0$  at 2 K.

i.e., below  $T_N$ , a clear hysteresis is seen for  $x = 0.05$  with  $M(0) \sim 1.69$  emu  $\text{g}^{-1}$ , whereas  $x = 0.10$  sample shows a very weak residual hysteresis up to magnetic field of 1.5 kOe with  $M(0) = 0.032$  emu  $\text{g}^{-1}$  only. Both samples show a linear  $M(H)$  behavior in the high-magnetic field region up to 20 kOe, a typical signature of a canted AFM. For both the samples,  $M(H)$  well above  $T_N$  is found to be linear over the whole measured magnetic field range.  $\mu_{\text{eff}}$  is found to be  $2.04 \mu_B$  per Cu ion for  $x = 0.10$ . This small increase in  $\mu_{\text{eff}}$  for  $x = 0.10$  with respect to  $x = 0.05$  ( $1.95 \mu_B$  per Cu ion) may be due to the presence of larger fraction of spin-3/2  $\text{Co}^{2+}$  ions.  $\theta$  does not change much from  $x = 0.05$  ( $-59.9$  K) to  $x = 0.10$  ( $-58.28$  K) in consistent with the result of small reduction in their  $T_N$  (30.3 K for  $x = 0.05$  to 29.5 K for  $x = 0.10$ ).  $\text{Co}_2\text{V}_2\text{O}_7$ , on the other hand, shows a typical behavior of AFM with

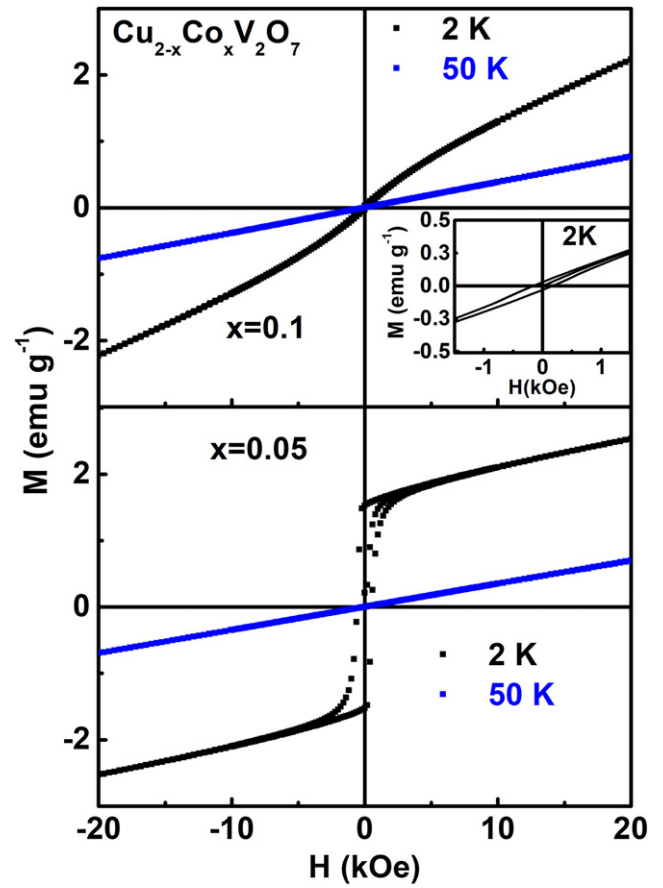


**Figure 8.** Field dependence of magnetization  $M$  of  $\text{Cu}_{2-x}\text{Co}_x\text{V}_2\text{O}_7$  for  $x = 0.05$  and  $x = 0.10$ . Inset shows the magnified low-field part for  $x = 0.10$  showing the presence of a residual FM phase.

$T_N = 10$  K (figure 7) which is in agreement with the previous studies [26, 31]. Below  $T_N$ ,  $M(H)$  exhibits linear behavior as shown in the inset of figure 7 (first quadrant only).  $\mu_{\text{eff}}$  is found to be  $3.27 \mu_B$  per  $\text{Co}^{2+}$  ion which is slightly smaller than the spin only value,  $\mu_{\text{eff}} = g\mu_B\sqrt{S(S+1)} = 3.87 \mu_B$  ( $g = 2$  and  $S = \frac{3}{2}$ ). So, a strong suppression of ferromagnetism in  $\text{Cu}_{2-x}\text{Co}_x\text{V}_2\text{O}_7$  with Co doping is observed before  $\alpha$ - to  $\beta$ -phase transition point ( $x_c = 0.15$ ) is reached, a result, very different from Mg- and Zn-doped  $\alpha$ - $\text{Cu}_2\text{V}_2\text{O}_7$ . The observed behavior may be attributed to the disorder created in the magnetic spin structure of  $\alpha$ - $\text{Cu}_2\text{V}_2\text{O}_7$  by spin- $\frac{3}{2}$   $\text{Co}^{2+}$  while replacing spin- $\frac{1}{2}$   $\text{Cu}^{2+}$ .

### 3.3. Heat capacity and magnetic entropy

The temperature dependence of heat capacity  $C_p$  for  $\text{Cu}_{2-x}\text{Mg}_x\text{V}_2\text{O}_7$  with  $x = 0.15$  and  $0.30$  is shown in figure 9(a). Clear evidence of magnetic ordering is noticed around 26 K and 21.5 K for  $x = 0.15$  and  $0.30$ , respectively. It is well known that in a magnetic insulator,  $C_p$  consists of two major parts: one from lattice and another from spin. The high-temperature part is dominated by phonon contribution while the low-temperature part is dominated by magnetic contribution. To estimate the magnetic contribution  $C_m(T)$  to the heat capacity, the high-temperature data have been fitted with the Debye–Einstein model as shown in figure 9(a). In this way,

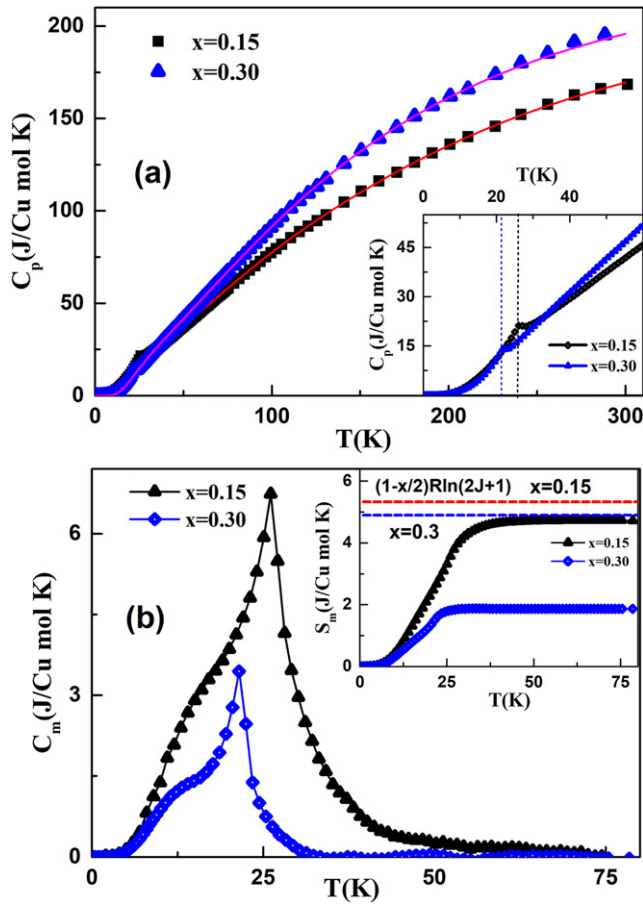


**Figure 9.** (a) Temperature dependence of heat capacity  $C_p$  of  $\text{Cu}_{2-x}\text{Mg}_x\text{V}_2\text{O}_7$  for  $x = 0.15$  and  $0.30$ . The solid line represents the lattice contribution ( $C_L$ ) to the heat capacity obtained by fitting the high temperature data with the Debye–Einstein model. Inset shows the magnified low temperature part showing clear evidence of magnetic ordering around 26 K and 21.5 K for  $x = 0.15$  and  $0.30$ , respectively. (b) The magnetic contribution to the heat capacity  $C_m(T)$  of  $\text{Cu}_{2-x}\text{Mg}_x\text{V}_2\text{O}_7$  for  $x = 0.15$  and  $0.30$  samples in the temperature range 2–75 K. The inset shows the magnetic entropy ( $S_m$ ) as a function of temperature, and the dotted lines denote the theoretical values of the entropy  $[(1 - \frac{x}{2})R \ln(2J + 1)]$  for  $\text{Cu}_{2-x}\text{Mg}_x\text{V}_2\text{O}_7$  with Cu spin  $S = \frac{1}{2}$ .

one can approximate the lattice contribution  $C_L(T)$ . The high-temperature fit has been extrapolated down to low temperature and  $C_m(T)$  has been estimated by subtracting  $C_L(T)$  from  $C_p(T)$ . Figure 9(b) shows  $C_m(T)$  for both the samples, indicating clearly the evidence of long-range ordering at low temperature, in consistent with the magnetization data. We have also calculated the magnetic entropy using the expression,

$$S_m(T) = \int_0^T \frac{C_{\text{mag}}(T)}{T} dT. \quad (2)$$

The plot of  $S_m(T)$  is shown in the inset of figure 9(b). The estimated high-temperature saturation value of  $S_m(T)$  for  $x = 0.15$  is found to be  $\sim 4.73$  J/Cu mol K, lower than the theoretical value  $5.33$  J/Cu mol K  $[(1 - \frac{x}{2})R \ln(2J + 1)]$  for  $\text{Cu}_{2-x}\text{Mg}_x\text{V}_2\text{O}_7$  with Cu spin  $S = \frac{1}{2}$ . But  $S_m$  for  $x = 0.30$  is drastically reduced to  $1.87$  J/Cu mol K. This result suggests that the number of spins taking part in long-range magnetic

ordering is significantly small and decreases rapidly with Mg doping.

### 3.4. Dielectric properties

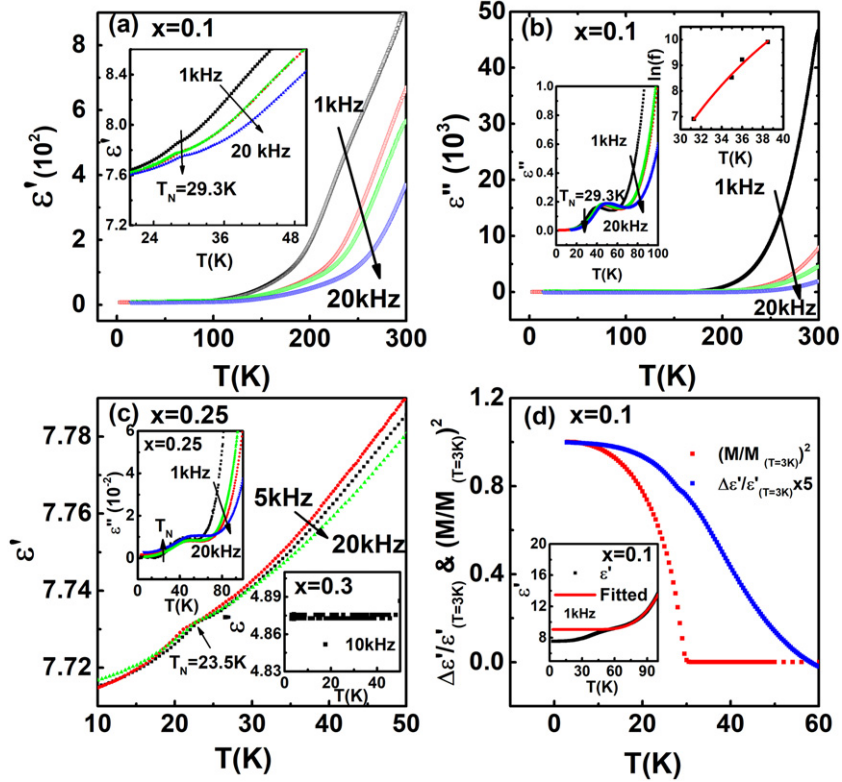
Since it is already known that  $\alpha\text{-Cu}_2\text{V}_2\text{O}_7$  is a multiferroic [9, 11], here we are primarily interested in examining how the ME properties change due to doping of non-magnetic Mg at the Cu site. The variation of real ( $\epsilon'$ ) and imaginary ( $\epsilon''$ ) part of dielectric constant with temperature (3–300 K) and frequency in the range 1–20 kHz for  $\text{Cu}_{2-x}\text{Mg}_x\text{V}_2\text{O}_7$  ( $x = 0.10, 0.25$  and  $0.30$ ) are shown in figures 10(a), (b) and (c). It is apparent that for all the compositions,  $\epsilon'$  depends weakly on the frequency at low temperature (figures 10(a) and (c)). But as temperature increases beyond 100 K, irrespective of composition,  $\epsilon'$  increases and shows a frequency dispersion. With the increase in frequency,  $\epsilon'$  decreases, which is a typical characteristic of most of the polar dielectrics. If one examines critically the low-temperature part of  $\epsilon'(T)$  curve, an anomaly is observed for compositions up to  $x = 0.25$  around their corresponding  $T_N$  (figures 10(a) and (c)). However, the anomaly loses its prominence as Mg concentration increases. We have not observed any anomaly at  $T_N$  for  $x \geq 0.30$  (lower inset of figure 10(c)). This result may be due to the existence of ME coupling up to  $x = 0.25$  associated with the NCSM crystal structure.

Figure 10(b) shows temperature variation of  $\epsilon''$  at different frequencies for  $x = 0.10$  sample. Apparently,  $\epsilon''$  is small below 200 K but increases rapidly above 200 K. This increasing trend in  $\epsilon''$  in the high-temperature region may be due to the space charge polarization.  $\epsilon''$  vs  $T$  for all the samples up to  $x = 0.25$  shows similar behavior. However, a closer observation reveals a broad peak in the low-temperature region for all the samples up to  $x = 0.25$ . Moreover, this peak shifts toward the higher temperature side with increasing frequency as shown in the insets of figures 10(b) and (c). Generally, one observes the signature of relaxor FE like behavior through the appearance of a broad peak in the temperature dependence of relative dielectric permittivity, extending over a finite temperature range. Like many other relaxor FEs, the frequency dependence of the maximum of the  $\epsilon''$  vs  $T$  curve can be fitted well with the VF equation [48, 49] (as shown at the right inset of figure 10(b) for  $x = 0.1$ ),

$$f = f_0 e^{-\frac{E_a}{k(T_m - T_{vf})}}, \quad (3)$$

where  $T_m$  is the peak temperature of  $\epsilon''$  vs  $T$  curve for a particular frequency  $f$ ,  $f_0$  is the limiting response frequency of the dipoles,  $E_a$  is the activation energy and  $T_{vf}$  is the characteristic VF freezing temperature and  $k$  is the Boltzmann constant. A finite non-zero freezing temperature ( $T_{vf} = 6.5$  K for  $x = 0.1$ ) is physically reasonable (although rather lower than most of the relaxor FEs but not very unusual) and in good agreement with  $\text{BaZr}_{1-x}\text{Ti}_x\text{O}_3$  relaxor system [50]. Moreover, the activation energy ( $\sim 29$  meV) is also of the same order of magnitude as observed in  $\text{BaZr}_{1-x}\text{Ti}_x\text{O}_3$  solid solution. So, the nature of  $\epsilon''$  vs  $T$  curve in the temperature range between 30 and 40 K indicates relaxor FE kind behavior.

To explain the origin of the anomaly in  $\epsilon'$  appearing at  $T_N$  for the undoped  $\alpha\text{-Cu}_2\text{V}_2\text{O}_7$ , we have used the Landau theory



**Figure 10.** Temperature dependence of the (a) real part ( $\epsilon'$ ) and (b) imaginary part ( $\epsilon''$ ) of dielectric constant of  $\text{Cu}_{2-x}\text{Mg}_x\text{V}_2\text{O}_7$  for  $x = 0.10$ . Left inset shows the magnified low temperature part. Vogel–Fulcher (VF) relaxation dynamics is represented in the right inset. (c) Magnified low temperature part of  $\epsilon'$  of  $\text{Cu}_{2-x}\text{Mg}_x\text{V}_2\text{O}_7$  for  $x = 0.25$  indicating clearly the presence of humplike anomaly. The upper inset shows its ( $\epsilon' \sim T$ ) behavior in the low temperature region. Lower inset shows absence of any anomaly in  $\epsilon' \sim T$  behavior around  $T_N$  for  $x = 0.30$ . (d) Temperature variation of normalized  $\frac{\delta\epsilon'}{\epsilon'(3K)}$  and  $[\frac{M}{M(3K)}]^2$  of  $\text{Cu}_{2-x}\text{Mg}_x\text{V}_2\text{O}_7$  for  $x = 0.10$  showing the existence of non-linear ME coupling. Presence of dielectric anomaly is clearly visible in the inset and the curve is a fit to equation (3).

of continuous phase transition and have shown in our previous studies [9] that the ME coupling is non-linear [26, 51]. In this work, we have applied the same theory to ascertain whether it remains still valid for  $\text{Cu}_{2-x}\text{Mg}_x\text{V}_2\text{O}_7$  in the low-doped region where weak FM behavior is observed due to the presence of DM interaction. According to this theory, the thermodynamic potential  $\Phi$  can be expressed as [52, 53],

$$\Phi = \Phi_0 + c_1 P^2 + \frac{c_2}{2} P^4 - PE + c'_1 M^2 + \frac{c'_2}{2} M^4 - MH + \gamma P^2 M^2, \quad (4)$$

where  $\Phi_0$  is the reference potential,  $c_1, c_2, c'_1, c'_2$  are the functions which depend on temperature and the last term  $\gamma P^2 M^2$  represents the ME coupling. Around the magnetic transition temperature, the change in dielectric constant  $\epsilon'$  can be taken to be proportional to  $\partial^2 \Phi / \partial P^2$ . So, from the above equation one easily obtains  $\delta\epsilon' \propto \gamma M^2$ , i.e., change in  $\epsilon'$  is proportional to the square of the magnetization. In the paramagnetic state, to include the lattice contribution to the dielectric constant, we have fitted the  $\epsilon'$  vs  $T$  data for  $x = 0.10$  sample with the following equation [26, 51],

$$\epsilon'(T) = \epsilon'(0) + \frac{C_0}{\exp\left(\frac{\hbar\omega_0}{k_B T}\right) - 1}. \quad (5)$$

The anomaly in  $\epsilon'$  around  $T_N$  is clearly visible in the inset of figure 10(d) where the fitted curve has been plotted along with the experimental  $\epsilon'$  vs  $T$  data. To have an idea regarding the nature of the ME coupling even after Mg doping, we have first calculated  $\Delta\epsilon'$ , defined as the difference between experimental  $\epsilon'$  vs  $T$  data and the fitted data. Figure 10(d) shows that a more or less nonlinear, i.e.,  $\delta\epsilon' \propto \gamma M^2$  behavior is retained in  $x = 0.10$  sample [9, 26]. As compared to  $[\frac{M}{M(3K)}]^2$  vs  $T$  curve, normalized  $\frac{\delta\epsilon'}{\epsilon'(3K)}$  vs  $T$  curve is slightly flattened around the magnetic transition region. This may be due to the broad nature of the anomaly in  $\epsilon'(T)$  around  $T_N$  as compared to the undoped one.

In  $\text{Co}_2\text{V}_2\text{O}_7$ , a correlation between the dielectric constant and inverse magnetization has been observed [26]. We have already mentioned that the CSM crystal structure of  $\text{Co}_2\text{V}_2\text{O}_7$  does not allow a ME coupling by the same DM interaction mechanism as proposed for the NCSM  $\alpha\text{-Cu}_2\text{V}_2\text{O}_7$ . Furthermore, in  $\text{Cu}_{2-x}\text{Co}_x\text{V}_2\text{O}_7$ , the FM behavior associated with antisymmetric DM exchange interaction is very weak. For these reasons, we have focused only on the dielectric properties of NCSM  $\alpha\text{-Cu}_2\text{V}_2\text{O}_7$ .

### 3.5. Phase diagram

In order to understand the effect of different magnetic and non-magnetic dopants on magnetic properties of

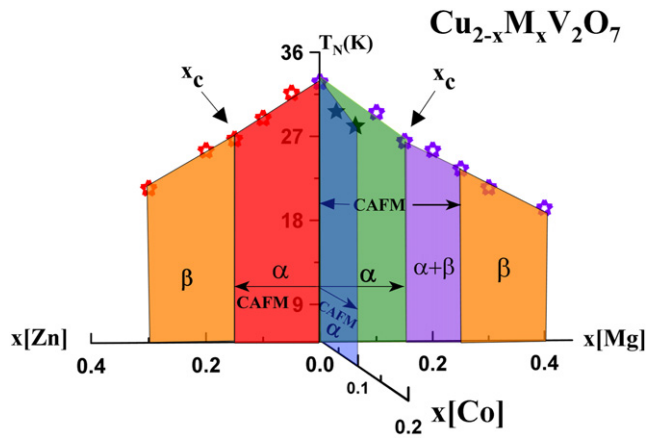


**Figure 11.** Combined magnetic phase diagram for  $\text{Cu}_{2-x}\text{M}_x\text{V}_2\text{O}_7$  ( $M = \text{Mg}, \text{Zn}$  and  $\text{Co}$ ) showing a linear decrease in magnetic transition temperature with dopant concentration. Green followed by purple and orange regions shows how the  $\alpha$ - and  $\beta$ -phases evolve with Mg doping. Red followed by orange region shows evolution of  $\alpha$ - and  $\beta$ -phases with Zn doping. Blue region indicates existence of  $\alpha$ -phase in magnetic Co-doped  $\text{Cu}_2\text{V}_2\text{O}_7$ .  $x_c$  denotes the critical doping concentration beyond which the transition from  $\alpha$ - to  $\beta$ -phase occurs. CAFM denotes canted AFM where a weak ferromagnetism is observed due to DM interaction.

$\alpha$ - $\text{Cu}_2\text{V}_2\text{O}_7$ , we have constructed a combined phase diagram for  $\text{Cu}_{2-x}\text{Mg}_x\text{V}_2\text{O}_7$  for  $x$  up to 0.40 and  $\text{Cu}_{2-x}\text{Co}_x\text{V}_2\text{O}_7$  for  $x$  up to 0.10, by plotting the magnetic transition temperature as a function of dopant concentration in figure 11. This figure also includes data of  $\text{Cu}_{2-x}\text{Zn}_x\text{V}_2\text{O}_7$  for  $x$  up to 0.30, taken from reference [9]. Dielectric anomalies have also been observed around the magnetic transition in the NCSM  $\alpha$ -phase of both Zn- and Mg-doped compounds. Magnetic transition temperature shows almost linear decrease with dopant concentration for both types of doping, magnetic or non-magnetic. The rate of decrease is found to be similar for spin-0 Mg/Zn and spin- $\frac{3}{2}$  Co doping,  $\frac{dT_c}{dx} \sim 32.5$  K. In  $\text{Ni}_3\text{V}_2\text{O}_8$ , on the other hand, the rate of suppression in transition temperature on doping with spin- $\frac{3}{2}$  Co is found to be smaller as compared to spin-0 Zn [20].

Several recent studies indicate that a small difference in the crystal structure has a strong impact on magnetic properties of  $\text{Cu}_2\text{V}_2\text{O}_7$  [8, 9, 11]. The presence of DM interaction in the NCSM  $\alpha$ -phase leads to weak ferromagnetism, which is absent in CSM  $\beta$ -phase. DM interaction is basically written as  $H_{\text{DM}} = \sum_{ij} \vec{D}_{ij} \cdot (\vec{S}_i \times \vec{S}_j)$ , where  $\vec{S}_i$  and  $\vec{S}_j$  are NN spins and  $\vec{D}_{ij}$  is the DM vector whose strength and direction are determined by the symmetries of the magnetic material. Moriya figured out five useful rules to determine the direction of  $\vec{D}$  based on the symmetry arguments [54, 55]. For example, if a center of inversion is located at the midpoint of the line joining the two spins  $i$  and  $j$ , the DM vector is zero. Due to two asymmetric exchange paths in the  $\alpha$ -phase, two non-compensating DM vectors arise, and as a result, a net DM interaction is induced. However, DM vectors cancel each other due to the symmetric exchange paths in the  $\beta$ -phase, and thereby, the DM interaction is absent in this phase.

The  $\alpha$ - to  $\beta$ -phase transition in  $\alpha$ - $\text{Cu}_2\text{V}_2\text{O}_7$  with Mg/Co doping can be explained in the following way. As  $\text{Cu}^{2+}$  is a Jahn–Teller (JT) active ion, the  $\text{CuO}_5$  polyhedra in  $\alpha$ - $\text{Cu}_2\text{V}_2\text{O}_7$  are elongated. However,  $\text{Mg}^{2+}$  is not JT active and the JT effect is not pronounced in  $\text{Co}^{2+}$  ion due to its high-spin  $3d^7$  configuration. With the increase of  $\text{Mg}^{2+}/\text{Co}^{2+}$ , the shortening of the apical  $M$ –O ( $M = \text{Cu}, \text{Mg}, \text{Co}$ ) bond and the elongation of the equatorial  $M$ –O bonds may occur. Thus, the overall distorted nature of the  $\text{MO}_5$  polyhedra is suppressed gradually due to the increasing presence of the regular  $\text{MgO}_5/\text{CoO}_5$  polyhedra. This triggers the transition from NCSM  $\alpha$ - to CSM  $\beta$ -phase around a critical concentration  $x_c = 0.15$  as also seen in  $\text{Cu}_{2-x}\text{Zn}_x\text{V}_2\text{O}_7$  [8, 9]. Recent DFT studies have reported that the dominant exchange interaction in  $\alpha$ - $\text{Cu}_2\text{V}_2\text{O}_7$  is between the third NN spins, which together with appreciable DM interaction make the  $\alpha$ -phase more like a three-dimensional (3D) spin system [30]. Our magnetic studies reveal that interchain coupling  $J_{\text{inter}}$  in  $\text{Cu}_{2-x}\text{Mg}_x\text{V}_2\text{O}_7$  is significant, and it decreases slowly with Mg concentration. These findings are in line with the above-mentioned DFT results.

#### 4. Summary

We have investigated the effect of non-magnetic Mg and magnetic Co doping on  $\alpha$ - $\text{Cu}_2\text{V}_2\text{O}_7$  using structural, magnetic, heat capacity, and dielectric measurements. Mg doping introduces an onset of a structural phase transition from an NCSM  $\alpha$ -phase to a CSM  $\beta$ -phase around a critical Mg concentration  $x_c = 0.15$ , the same concentration as observed in the similar Zn-doped system. But in the Mg-doped system,  $\alpha$ -phase continues to exist up to  $x = 0.25$  in a small percentage. As a result of Mg doping, the dielectric anomaly as seen around the magnetic transition temperature for undoped  $\alpha$ - $\text{Cu}_2\text{V}_2\text{O}_7$  gradually loses its prominence but exists up to  $x = 0.25$ . On the other hand, Co doping triggers a sharp  $\alpha$ - to  $\beta$ -phase transition around the same doping concentration  $x_c = 0.15$ . So,  $x_c = 0.15$  doping concentration seems to be independent of the type of doping, magnetic or non-magnetic. The magnetic phase diagram demonstrates that the rate of suppression of  $T_N$  with Mg and Co doping is the same. Finally, the present study explores the possibility of controlling the magnetic and dielectric properties of Cu-based divanadates by doping with judiciously selected magnetic or nonmagnetic ions at least over a limited composition range.

#### Acknowledgments

This work has been supported by the Science and Engineering Research Board (SERB), Government of India (Grant No. EMR/2016/006295). Abja Keshar Kar gratefully acknowledges a fellowship from SERB, India. DM acknowledges the funding from the Technical Research Center, Department of Science and Technology, Government of India (Grant No. AI/1/62/IACS/2015) and SERB, Government of India (Grant No. SRG/2019/000387).

## Data availability statement

All data that support the findings of this study are included within the article (and any supplementary files).

## ORCID iDs

Bidisa Chattopadhyay  <https://orcid.org/0000-0002-0288-1492>

Md A Ahmed  <https://orcid.org/0000-0002-3529-5123>

D Jana  <https://orcid.org/0000-0002-7651-1355>

Prabhat Mandal  <https://orcid.org/0000-0002-0672-0901>

## References

- [1] Dzyaloshinskii I 1958 A thermodynamic theory of weak ferromagnetism of antiferromagnetics *J. Phys. Chem. Solids* **4** 241
- [2] Moriya T 1960 Anisotropic superexchange interaction and weak ferromagnetism *Phys. Rev.* **120** 91
- [3] Kimura T, Goto T, Shintani H, Ishizaka K, Arima T and Tokura Y 2003 Magnetic control of ferroelectric polarization *Nature* **426** 55
- [4] Auciello O, Scott J F and Ramesh R 1998 The physics of ferroelectric memories *Phys. Today* **51** 22
- [5] Kumar A, Ortega N, Dussan S, Kumari S, Sanchez D, Scott J and Katiyar R 2012 Multiferroic memory: a disruptive technology or future technology? *Solid State Phenom.* **189** 1
- [6] Nan C-W, Bichurin M I, Dong S, Viehland D and Srinivasan G 2008 Multiferroic magnetoelectric composites: historical perspective, status, and future directions *J. Appl. Phys.* **103** 031101
- [7] Tokura Y, Seki S and Nagaosa N 2014 Multiferroics of spin origin *Rep. Prog. Phys.* **77** 076501
- [8] Pommer J, Kataev V, Choi K-Y, Lemmens P, Ionescu A, Pashkevich Y, Freimuth A and Güntherodt G 2003 Interplay between structure and magnetism in the spin-chain compound  $(\text{Cu, Zn})_2\text{V}_2\text{O}_7$  *Phys. Rev. B* **67** 214410
- [9] Chattopadhyay B, Ahmed M A, Bandyopadhyay S, Singha R and Mandal P 2017 Magnetic ordering induced ferroelectricity in  $\alpha\text{-Cu}_2\text{V}_2\text{O}_7$  studied through nonmagnetic Zn doping *J. Appl. Phys.* **121** 094103
- [10] Aguilar R V, Mostovoy M, Sushkov A B, Zhang C L, Choi Y J, Cheong S-W and Drew H D 2009 Origin of electromagnon excitations in multiferroic  $\text{RMnO}_3$  *Phys. Rev. Lett.* **102** 047203
- [11] Sannigrahi J, Bhowal S, Giri S, Majumdar S and Dasgupta I 2015 Exchange–striction induced giant ferroelectric polarization in copper-based multiferroic material  $\alpha\text{-Cu}_2\text{V}_2\text{O}_7$  *Phys. Rev. B* **91** 220407(R)
- [12] Lee Y-W, Jang T-H, Dissanayake S E, Lee S and Jeong Y H 2016 Magnetism and magnetoelectricity in the polar oxide  $\alpha\text{-Cu}_2\text{V}_2\text{O}_7$  *Europhys. Lett.* **113** 27007
- [13] Shirolkar M M, Hao C, Dong X, Guo T, Zhang L, Li M and Wang H 2014 Tunable multiferroic and bistable/complementary resistive switching properties of dilutely Li-doped  $\text{BiFeO}_3$  nanoparticles: an effect of aliovalent substitution *Nanoscale* **6** 4735
- [14] Tian Z M, Qiu Y, Yuan S L, Wu M S, Huo S X and Duan H N 2010 Enhanced multiferroic properties in Ti-doped  $\text{Bi}_2\text{Fe}_4\text{O}_9$  ceramics *J. Appl. Phys.* **108** 064110
- [15] Priyadharsini P, Pradeep A, Sathyamoorthy B and Chandrasekaran G 2014 Enhanced multiferroic properties in La and Ce co-doped  $\text{BiFeO}_3$  nanoparticles *J. Phys. Chem. Solids* **75** 797
- [16] Nayek C, Tamilselvan A, Thirimal C, Murugavel P and Balakumar S 2014 Origin of enhanced magnetization in rare earth doped multiferroic bismuth ferrite *J. Appl. Phys.* **115** 073902
- [17] Yu B, Li M, Liu J, Guo D, Pei L and Zhao X 2008 Effects of ion doping at different sites on electrical properties of multiferroic  $\text{BiFeO}_3$  ceramics *J. Phys. D: Appl. Phys.* **41** 065003
- [18] Kothari D, Raghavendra Reddy V, Gupta A, Meneghini C and Aquilanti G 2010 Eu doping in multiferroic  $\text{BiFeO}_3$  ceramics studied by Mossbauer and EXAFS spectroscopy *J. Phys.: Condens. Matter.* **22** 356001
- [19] Du Y, Cheng Z X, Wang X L and Dou S X 2010 Lanthanum doped multiferroic  $\text{DyFeO}_3$ : structural and magnetic properties *J. Appl. Phys.* **107** 09D908
- [20] Kumarasiri A and Lawes G 2011 Control of the multiferroic transition in  $\text{Ni}_3\text{V}_2\text{O}_8$  by transition metal doping *Phys. Rev. B* **84** 064447
- [21] Kumarasiri A, Abdelhamid E, Dixit A and Lawes G 2015 Effect of transition metal doping on multiferroic ordering in  $\text{FeVO}_4$  *Phys. Rev. B* **91** 014420
- [22] Liu J, Fang L, Zheng F, Ju S and Shen M 2009 Enhancement of magnetization in Eu doped  $\text{BiFeO}_3$  nanoparticles *Appl. Phys. Lett.* **95** 022511
- [23] Albaalbakky A, Kvashnin Y, Patte R, Frésard R and Ledue D 2018 Effects of Ga doping on magnetic and ferroelectric properties of multiferroic delafossite  $\text{CuCrO}_2$ : *ab initio* and Monte Carlo approaches *Phys. Rev. B* **98** 174403
- [24] Zhang Q, Knafo W, Adelman P, Schweiss P, Grube K, Qureshi N, Wolf T, Löhneysen H v and Meingast C 2011 Complex magnetoelastic properties in the frustrated kagome-staircase compounds  $(\text{Co}_{1-x}\text{Ni}_x)_3\text{V}_2\text{O}_8$  *Phys. Rev. B* **84** 184429
- [25] Kharel P, Kumarasiri A, Dixit A, Rogado N, Cava R J and Lawes G 2009 Scaling behaviour of magnetic transitions in  $\text{Ni}_3\text{V}_2\text{O}_8$  *Phil. Mag.* **89** 1923
- [26] Sánchez-Andújar M, Yáñez-Vilar S, Mira J, Biskup N, Rivas J, Castro-García S and Señaris-Rodríguez M A 2011 Role of the magnetic ordering on the dielectric response of  $\text{M}_2\text{V}_2\text{O}_7$  ( $\text{M} = \text{Co}$  and  $\text{Cu}$ ) divanadates *J. Appl. Phys.* **109** 054106
- [27] Chen R et al 2018 Magnetic field induced ferroelectricity and half magnetization plateau in polycrystalline  $\text{R}_2\text{V}_2\text{O}_7$  ( $\text{R} = \text{Ni, Co}$ ) *Phys. Rev. B* **98** 184404
- [28] Ji W H et al 2019 Noncollinear magnetic structure and anisotropic magnetoelastic coupling in cobalt pyrovanadate  $\text{Co}_2\text{V}_2\text{O}_7$  *Phys. Rev. B* **100** 134420
- [29] Gitgeatpong G, Zhao Y, Avdeev M, Piltz R O, Sata T J and Matan K 2015 Magnetic structure and Dzyaloshinskii-Moriya interaction in the  $S = 1/2$  helical-honeycomb antiferromagnet  $\alpha\text{-Cu}_2\text{V}_2\text{O}_7$  *Phys. Rev. B* **92** 024423
- [30] Gitgeatpong G et al 2017 High-field magnetization and magnetic phase diagram of  $\alpha\text{-Cu}_2\text{V}_2\text{O}_7$  *Phys. Rev. B* **95** 245119
- [31] Sannigrahi J, Giri S and Majumdar S 2017 Observation of weak ferromagnetism and the sizable magnetocaloric effect in  $\text{Co}_2\text{V}_2\text{O}_7$  *J. Phys. Chem. Solids* **101** 1
- [32] Yin L, Ouyang Z W, Wang J F, Yue X Y, Chen R, He Z Z, Wang Z X, Xia Z C and Liu Y 2019 Anisotropic magnetization plateaus in  $S_{\text{eff}} = 1/2$  skew-chain single-crystal  $\text{Co}_2\text{V}_2\text{O}_7$  *Phys. Rev. B* **99** 134434
- [33] Tena M A and Garcia-Granda S 2015 Structural characterization and colour of  $\text{Mg}_x\text{Cu}_{3-x}\text{V}_2\text{O}_8$  ( $0 \leq x \leq 3$ ) and  $\text{Mg}_y\text{Cu}_{2-y}\text{V}_2\text{O}_7$  ( $0 \leq y \leq 2$ ) compositions *Springer Plus* **4** 163
- [34] Shannon R D 1976 Revised effective ionic radii and systematic studies of interatomic distances in halides and chalcogenides *Acta Crystallogr. A* **32** 751
- [35] Banerjee A, Sannigrahi J, Bhowal S, Dasgupta I, Majumdar S, Walker H C, Bhattacharyya A and Adroja D T 2016 Spin

- wave excitations in the pyrovanadate  $\alpha$ - $\text{Cu}_2\text{V}_2\text{O}_7$  *Phys. Rev. B* **94** 144426
- [36] Zhang J T, Wang J L, Ji C, Guo B X, Xia W S, Lu X M and Zhu J S 2017 Magnetism and spin-driven ferroelectricity in the multiferroic material  $\alpha$ - $\text{Cu}_2\text{V}_2\text{O}_7$  *Phys. Rev. B* **96** 165132
- [37] Blundell S 2001 *Magnetism in Condensed Matter* (Oxford: Oxford University Press)
- [38] Nicholls D 1974 *Manganese Complexes and First-Row Transition Elements (A Macmillan Chemistry Text)* (London: Palgrave)
- [39] Bonner J C and Fisher M E 1964 Linear magnetic chains with anisotropic coupling *Phys. Rev.* **135** A640
- [40] Venkatesh C, Bandyopadhyay B, Midya A, Mahalingam K, Ganesan V and Mandal P 2020 Magnetic properties of the one-dimensional  $S = 3/2$  Heisenberg antiferromagnetic spin-chain compound  $\text{Na}_2\text{M}_3\text{O}_7$  *Phys. Rev. B* **101** 184429
- [41] He Z and Ueda Y 2008 Paramagnetic anisotropy and spin-flop transition in single crystals of the quasi-one-dimensional system  $\beta$ - $\text{Cu}_2\text{V}_2\text{O}_7$  *Phys. Rev. B* **77** 052402
- [42] Touaiher M, Rissouli K, Benkhoucha K, Taibi M, Aride J, Boukhari A and Heulin B 2004 Crystal structures and magnetic properties of  $M_2\text{V}_2\text{O}_7$  ( $M = \text{Co}, \text{Ni}$  and  $\text{Cu}$ ) compounds *Mat Mater. Chem. Phys.* **85** 41
- [43] Tsirlin A A, Janson O and Rosner H 2010  $\beta$ - $\text{Cu}_2\text{V}_2\text{O}_7$ : a spin-1/2 honeycomb lattice system *Phys. Rev. B* **82** 144416
- [44] Ruan M Y, Ouyang Z W, Sun Y C, Xia Z C, Rao G H and Chen H S 2017 Examining magnetic models and anisotropies in  $\beta$ - $\text{Cu}_2\text{V}_2\text{O}_7$  by high-frequency ESR *Appl. Magn. Reson.* **48** 423
- [45] de Jongh L J and Miedema A R 1974 Experiments on simple magnetic model systems *Adv. Phys.* **23** 1
- [46] Vasil'ev A N, Ponomarenko L A, Manaka H, Yamada I, Isobe M and Ueda Y 2001 Magnetic and resonant properties of quasi-one-dimensional antiferromagnet  $\text{LiCuVO}_4$  *Phys. Rev. B* **64** 024419
- [47] Tsukada I, Sasago Y, Uchinokura K, Zheludev A, Maslov S, Shirane G, Kakurai K and Ressouche E 1999  $\text{BaCu}_2\text{Si}_2\text{O}_7$ : a quasi-one-dimensional  $S = 1/2$  antiferromagnetic chain system *Phys. Rev. B* **60** 6601
- [48] Vogel H 1921 The temperature dependence law of the viscosity of fluids *Physikalische Zeitschrift* **22** 645
- [49] Fulcher G S 1925 Analysis of recent measurements of the viscosity of glasses *J. Am. Ceram. Soc.* **8** 339
- [50] Maiti T, Guo W R and Bhalla A S 2008 *J. Am. Ceram. Soc.* **91** 1769
- [51] Fox D L, Tilley D R, Scott J F and Guggenheim H J 1980 Magnetolectric phenomena in  $\text{BaMnF}_4$  and  $\text{BaMn}_{0.99}\text{Co}_{0.01}\text{F}_4$  *Phys. Rev. B* **21** 2926
- [52] Wang K F, Liu J-M and Ren Z F 2009 Multiferroicity: the coupling between magnetic and polarization orders *Adv. Phys.* **58** 321
- [53] Yang Y, Liu J-M, Huang H B, Zou W Q, Bao P and Liu Z G 2004 Magnetolectric coupling in ferroelectromagnet  $\text{Pb}(\text{Fe}_{1/2}\text{Nb}_{1/2})\text{O}_3$  single crystals *Phys. Rev. B* **70** 132101
- [54] Moriya T 1960 New mechanism of anisotropic superexchange interaction *Phys. Rev. Lett.* **4** 228
- [55] Dong S, Xiang H and Dagotto E 2019 Magnetolectricity in multiferroics: a theoretical perspective *Natl Sci. Rev.* **6** 629